IEEE Access
Multidisciplinary | Rapid Review | Open Access Journal

Received June 14, 2019, accepted July 19, 2019, date of publication July 23, 2019, date of current version August 9, 2019.

Digital Object Identifier 10.1109/ACCESS.2019.2930543

An Investigation Study on Mode Mixing Separation in Empirical Mode Decomposition

HAN-PING HUANG[1], SUNG-YANG WEI[1], HSUAN-HAO CHAO[1], CHANG FRANCIS HSU[1], LONG HSU[1], AND SIEN CHI[2]

[1]Department of Electrophysics, College of Science, National Chiao Tung University, Hsinchu 300, Taiwan
[2]Department of Photonics, College of Electrical and Computer Engineering, National Chiao Tung University, Hsinchu 300, Taiwan

Corresponding author: Sien Chi (schi@mail.nctu.edu.tw)

This work was supported by the Ministry of Science and Technology (MOST) of Taiwan under Grant MOST 107-2221-E-009-016.

ABSTRACT Mode mixing is a limitation of the empirical mode decomposition (EMD) method appropriate for physiological signal analysis. In 2008, boundary condition map presented by Rilling and Flandrin provided the efficiency of separating the two components of a two-tone signal as a function of their amplitude and frequency ratios. Until 2019, their findings were still applied. However, their maps only give an uncertainty-like efficiency of mode mixing separation for two-tone signals. In this paper, we propose a criterion for mode mixing separation in EMD, which provides a binary judgment on mode mixing separation instead of the above-mentioned efficiency. By comparing the slopes of the two components, we found that the phenomenon of mode mixing occurs as the extrema of the high-tone component are suppressed by the low-tone component. Under this condition, the criterion shows the relation among their amplitude ratio, frequency ratio, and relative phase between the two components. Given with the values of the three parameters, one can affirm whether the two components are mixed according to the criterion. Accordingly, we derive a black/white three-dimensional (3D) map that plots the binary result of mode mixing in black or white as a function of the three parameters. Our map agrees with Rilling's map and the results obtained from our gait analysis. Among the 23 sets of center-of-mass trajectory signals, six sets encountered the mode mixing problem and their coordinates of the three parameters were found in the black region of the map, while the other 17 sets were in the white region.

INDEX TERMS Empirical mode decomposition, mode mixing separation, improved EMD.

I. INTRODUCTION

Gait analysis is a method for identifying biomechanical abnormalities in the gait cycle. Traditionally, the gait stability of a patient is assessed via image processing from the trajectories of the markers attached on the body of the patient walking down a catwalk or a treadmill in a laboratory [1]–[3]. Alternatively, a relatively simple and inexpensive method was developed for the ambulatory assessment of center-of-mass (CoM) displacements by using inertial sensors [4], [5]. In this case, the acceleration signal acquired from an accelerometer was integrated with respect to time twice into a displacement time series. Usually, the noises hidden within a physiological signal can be filtered off by using the empirical mode decomposition (EMD) method [6]–[9], an adaptive filtering technique appropriate for physiological signal analysis. However, in our study of CoM trajectory, the EMD-based filtering technique failed occasionally.

The EMD method is a powerful signal analysis technique for nonstationary and nonlinear systems. The algorithm of the EMD is adaptive and data-driven, which decomposes a time series of multiple frequencies into a finite number of components through a sifting process in the time domain. Typically, each component, referred to as an intrinsic mode function (IMF) [6], [7], follows a trend characterized by a dominant frequency, which usually varies with time. This resembles the feature of nonstationary and nonlinear systems, including many physiological signals,

The associate editor coordinating the review of this manuscript and approving it for publication was Qinghua Guo

such as heart rate, respiratory rate, and stride rate. Thus, the EMD method is especially suitable for physiological signal analysis [10], [11].

For example, the CoM trajectory in the medio-lateral (ML) direction of a healthy adult during walking usually oscillates around 1 Hz statistically. This implies that an IMF with a dominant frequency of 1 Hz is expected among the various IMFs decomposed from a displacement time series. Indeed, in our gait analysis of 23 sets of CoM displacement signals, such a unique IMF could be extracted from 17 sets. However, it disappeared and remained mixed within other IMFs for the other six sets. When the phenomenon of mode mixing [12]–[14] occurs, the IMFs can lose their physical meaning, hindering the interpretation of the results of the analysis [6], [15]. Therefore, understanding the core cause of mode mixing in EMD will benefit mode mixing separation [16]–[22].

Mode mixing is a limitation of the EMD method [16]–[18]. It is caused by the presence of either temporal intermittence in a signal or closely spaced spectral components [15]. In 2008, Rilling and Flandrin explored a theoretical analysis that simulated the mode mixing in EMD in the case of a two-tone composite signal composed of two sinusoidal components of different frequencies [17]. They presented a *Boundary Condition Map*, which illustrates the efficiency of separating the two components as a function of their amplitude ratio and frequency ratio. Till 2019, their findings were still applied [15], [19]–[24]. However, each efficiency on the *Boundary Condition Map* was obtained as an average value over all relative phases of the criterion.

In this paper, based on the findings by Rilling and Flandrin [17], we further explored the core cause of the mode mixing separation of a two-tone signal, including the effect of the relative phase between the two tones. By using a similar concept [17] but from a different perspective, we propose a criterion for mode mixing separation in EMD, which provides a binary judgment instead of the above efficiency. In the following sections, it will be shown that, given with the amplitude ratio, the frequency ratio, and the relative phase between the two components of a two-tone signal, one can affirm whether the two components are mixed or not according to the criterion. Accordingly, a black/white 3D map is derived, which plots the binary result of mode mixing in black or white as a function of the three parameters. Theoretically, our map will be compared with Rilling's *Boundary Condition Map*. Experimentally, the judgment of mode mixing for each of the 23 sets of CoM signals obtained from our gait analysis will be confirmed with the aid of the black/white 3D map.

II. THEORY

A. MODE MIXING IN EMD

The EMD method decomposes a time series $x(t)$ into a finite number of components in the time domain. As a consequence, the target series can be rewritten in the form of $x(t) = \sum_{i=1}^{K} IMF_i(t) + r(t)$, where $IMF_i(t)$ is the i^{th} component

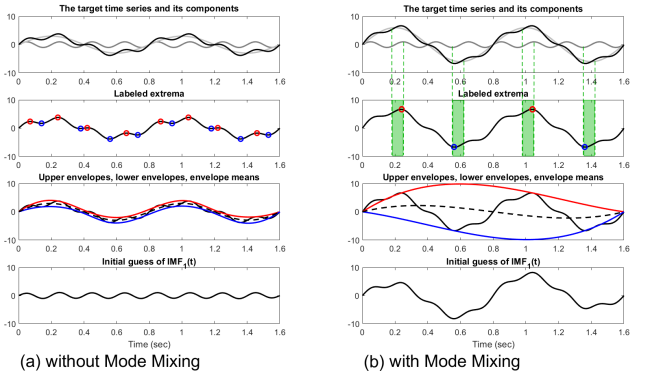

FIGURE 1. First sifting process of EMD for two different target time series (a) without and (b) with mode mixing, separately. These figures present the way in which the extrema affect the decomposition during the sifting process. Each target time series is composed of two sinusoidal functions whose frequencies are 5 Hz and 1.25 Hz and amplitudes are (a) 1 and 3 as well as (b) 1 and 6, respectively. The first panel shows the target time series (black) and its components (gray). The second panel identifies the local maxima (red circles) and local minima (blue circles). The third panel illustrates the upper envelope (red line) and lower envelope (blue line) and their mean (black dashed line). The last panel shows the difference between the target time series and the mean, which is the initial guess of IMF_1. In the presence of mode mixing, as shown in (b), each extremum of $x(t)$ lies within a single green region.

of the IMFs decomposed from $x(t)$, k is the total number of IMFs, and $r(t)$ is the residual trend. The EMD algorithm is a sifting process. The details of EMD can be found in [6], [25], [26]. It is worth noting that the key step in the sifting process is the identification of all extrema (local maxima and minima) of the target time series. Accordingly, each of the IMFs can be sequentially extracted, regardless of whether mode mixing occurs.

For example, Fig. 1 illustrates a typical sifting round of the EMD method for two target time series with and without mode mixing, separately. Both target series are two-tone composites and look alike. The high-tone components are the same, whereas the low-tone components are different only in amplitude. In the case of Fig. 1(a), 16 extrema are identified. Then, the interpolation of the eight local maxima splines an upper envelope, whereas that of the eight local minima splines a lower envelope. The mean of the two envelopes, denoted with a dashed line, reveals a low frequency similar to that of the low-tone component of the target series. Thus, subtracting the mean from the target series gives an initial guess of $IMF_1(t)$, which resembles the high-tone component of the target series. Under this condition, the two components are well separated from each other and mode mixing is absent.

On the contrary, in the case of Fig. 1(b), only four extrema are identified. The same process gives an initial guess of $IMF_1(t)$ similar to the original target series. In other words, mode mixing is present. Conceptually, this example illustrates the dependence of mode mixing in EMD on the number of extrema of the target series, which in turn is affected by the frequency ratio and the amplitude ratio of the two components [17], [27].

B. BOUNDARY CONDITION MAP

In the mode-mixing simulation for the *Boundary Condition Map* presented by Rilling and Flandrin [17] in 2008, a two-tone composite signal $x(t)$ was considered, which consisted of a low tone $F_L(t)$ and a high tone $F_H(t)$, as given by, respectively,

$$F_L(t) = a_L \times sin(2\pi f_L t + \varphi_L) \tag{1a}$$

and

$$F_H(t) = a_H \times sin(2\pi f_H t + \varphi_H), \tag{1b}$$

where a, f, and φ denote the amplitude, frequency, and initial phase of each of the two components and the subscripts L and H denote the low and high tones. Herein, $f_L < f_H$. They proposed an index of separation for the two-tone signal $x(t)$. The index measures the absolute value of the difference between the $IMF_1(t)$ extracted from $x(t)$ and the high tone $F_H(t)$, which is then normalized by the Euclidean norm of $F_H(t)$ over a certain period of time. The value of the index, depending on their amplitude and frequency ratios as well as their relative phase, ranges from zero to one. A zero value of the index indicates a perfect separation of the two tones while a value close to one implies a bad separation.

According to the index, they presented the 3D *Boundary Condition Map* which illustrates the efficiency of separating the two components of $x(t)$ as a function of their amplitude ratio a_L/a_H and frequency ratio f_L/f_H. Each efficiency on the *Boundary Map* was obtained as an average value over all relative phases of the index. The 2D projection of the 3D*Boundary Condition Map* onto the $(a_L/a_H, f_L f_H)$-plane of amplitude and frequency ratios exhibits three domains which are well separated by two boundary curves. The domain above the upper boundary curve, as given by the analytic expression $(a_L/a_H)(f_L/f_H)^2 = 1$, guarantees the presence of mode mixing within the area. On the contrary, the domain below the lower boundary curve, as given by a fit expression $(a_L/a_H)(f_L/f_H)sin(3\pi f_L/f_H/2) = 1$, guarantees the absence of mode mixing within the area. However, the domain in between is hybrid and the mode mixing performance of any $x(t)$ within the area is measured in terms of the separation efficiency ranging from zero to one. Although the lower boundary curve was modified by Feldman in 2009 [27] by treating the sifting process of EMD as a low pass filter, the hybrid domain still remains just with a smaller area.

It is worth pointing out that the index proposed by Rilling and Flandrin is indeed an uncertainty-like efficiency of separation of the two tones. Therefore, a criterion of mode mixing, which provides a binary judgment on the separation of the two components of a two-tone signal is desired.

C. CRITERION OF MODE MIXING IN EMD

In order to investigate the core cause of mode mixing in EMD, we also make use of the same two-tone composite signal $x(t)$. Recall that Fig. 1 illustrates the dependence of mode mixing in EMD on the number of extrema of the target signal $x(t)$. In order to identify all extrema of $x(t)$, we further derive the slopes or first derivatives of $F_L(t)$ and $F_H(t)$ with respect to time, as expressed in the forms of

$$m_L(t) = 2\pi f_L \times a_L \times cos(2\pi f_L t + \varphi_L) \tag{2a}$$

and

$$m_H(t) = 2\pi f_H \times a_H \times cos(2\pi f_H t + \varphi_H). \tag{2b}$$

The zero-crossings of $m_L(t)$ and $m_H(t)$ on the time axis locate the extrema of $F_L(t)$ and $F_H(t)$, respectively.

However, referring to Fig. 1, all the extrema of the two components $F_L(t)$ and $F_H(t)$ do not always contribute to the extrema of their composite $x(t)$. In the presence of mode mixing, as can be seen in Fig. 1(b), both the composite $x(t)$ and its low-tone component $F_L(t)$ contain an equal number of extrema. Careful examination of the top panel in Fig. 1(b) also reveals that the extrema of $x(t)$ and $F_L(t)$ appear in pairs but do not overlap. Each extremum of $x(t)$ is found lying between an extremum of $F_L(t)$ and a neighboring extremum of $F_H(t)$, as the region highlighted with a green background, where the signs of the two slopes $m_L(t)$ and $F_m(t)$ are opposite to each other. In order to suppress any more extrema protruded to $x(t)$ by the extrema of $F_H(t)$, only two kinds of relations between the slopes of $F_L(t)$ and $F_H(t)$ are allowed outside the green regions. One relation is that the signs of the two slopes $m_L(t)$ and $m_H(t)$ are the same. The other relation requires the magnitude of $m_H(t)$ be less than that of $m_L(t)$ over the intervals, denoted by $T_{opposite}$, in which the signs of the two slopes $m_L(t)$ and $m_H(t)$ are opposite to each other. The two relations between the slopes can be given by

$$\frac{|m_L(t)|}{|m_H(t)|} = -\frac{m_L(t)}{m_H(t)} > 1 \quad \text{for t} \in T_{opposite}. \tag{3}$$

Substituting (2a) for $m_L(t)$ and (2b) for $m_H(t)$ into (3) yields

$$\frac{a_L}{a_H} > -\frac{f_H \times cos(2\pi f_H t + \varphi_H)}{f_L \times cos(2\pi f_L t + \varphi_L)} \equiv M(t) > 0 \quad \text{for t} \in T_{opposite}, \tag{4}$$

where a_L/a_H is the amplitude ratio, f_L/f_H is the frequency ratio, and $M(t)$ is a new index that monitors the ratio of the slope of the low tone to that of the high tone with both at unit amplitude.

To characterize the new index $M(t)$, the top panel in Fig. 1(b) is further quantified for study. First, the low tone $F_L(t)$ and the high tone $F_H(t)$ are normalized to $F'_L(t) = sin(2\pi f_L t + \varphi_L)$ and $F'_H(t) = sin(2\pi f_H t + \varphi_H)$ of unit amplitude, respectively. Then, Figs. 2 and 3 plot the normalized $F'_L(t), F'_H(t)$, and their corresponding $M(t)$ as a function of time, separately, in which the parameters are set as follows: $f_H = 5\ Hz$, $f_L = 1.25\ Hz$, and $\varphi_L = 0$. For comparison, $\varphi_H = 0$ in Fig. 2 and $\varphi_H = \pi/2$ in Fig. 3. As expected in (4), the indices $M(t)$ in both figures are all greater than zero over the intervals $T_{opposite}$, highlighted with a gray background, in which the signs of the two slopes of $F'_L(t)$ and $F'_H(t)$ are

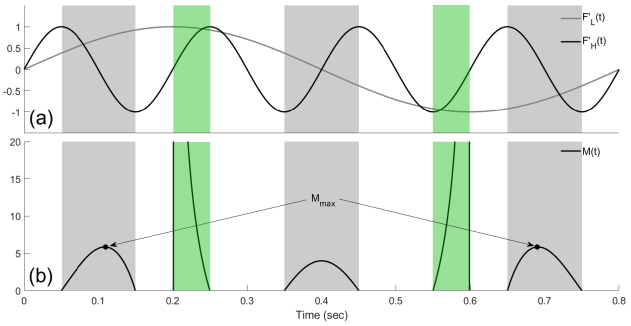

FIGURE 2. (a) $F_L'(t)$ and $F_H'(t)$ of unit-amplitude as well as (b) their corresponding $M(t)$ for the illustration of mode mixing separation according to the criterion given by (5). The parameters of $F_L'(t)$ and $F_H'(t)$ are set as $f_H = 5$ *Hz*, $f_L = 1.25$ *Hz*, $\varphi_L = 0$, and $\varphi_H = 0$. M_{max} in (b) is the maximum of $M(t)$ in the gray regions. For reference, a single extremum of $x(t)$ always exists in each of the green regions while no extrema of $x(t)$ are allowed in the white region. In the presence of mode mixing, not any extra extremum of $x(t)$ is allowed in the gray regions as the criterion is satisfied.

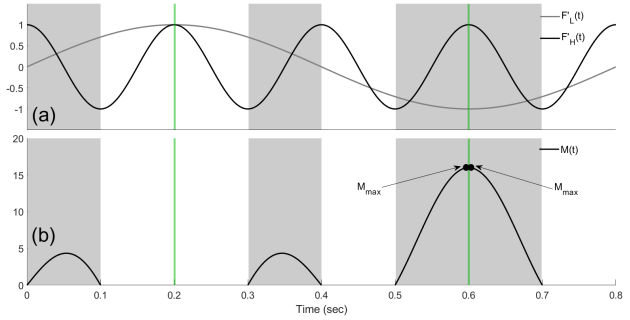

FIGURE 3. (a) $F_L'(t)$ and $F_H'(t)$ of unit-amplitude as well as (b) their corresponding $M(t)$ for the illustration of mode mixing separation according to the criterion given by (5). In this case: $f_H = 5$ *Hz*, $f_L = 1.25$ *Hz*, $\varphi_L = 0$, but $\varphi_H = \pi/2$. The green regions are shorten into individual green points. Two M_{max} points of a same value appear right beside the instance of the green point between two gray regions. For reference, a single extremum of $x(t)$ always exists in each of the green points while no extrema of $x(t)$ are allowed in the white region. In the presence of mode mixing, not any extra extremum of $x(t)$ is allowed in the gray regions as the criterion is satisfied.

opposite to each other. Thus, the requirement for a_L/a_H in (4) can be rewritten in the form of

$$a_L/a_H > M_{max} \quad \text{for t} \in T_{opposite}, \tag{5}$$

where M_{max} is the maximum of $M(t)$ within the gray regions, $t \in T_{opposite}$. Referring to Figs. 2 and 3, the expression in (5) indicates that, as the amplitude ratio a_L/a_H of the two original components $F_L(t)$ and $F_H(t)$ is greater than the maximum M_{max} of $M(t)$ over the gray regions, not any extra extremum will be contributed to $x(t)$ outside the green regions. Under this condition, $F_L(t)$ and $F_H(t)$ cannot be separated by EMD, and the phenomenon of mode mixing occurs. Therefore, (5) serves as a common criterion of mode mixing in EMD. Implicitly, the value of M_{max} in the criterion depends on the frequency ratio f_L/f_H, φ_H, and φ_L of the two tones and has to be solved numerically.

Nevertheless, the situation of $\varphi_H = \pi/2$ at $f_H = 5$ *Hz*, $f_L = 1.25$ *Hz*, and $\varphi_L = 0$ in Fig. 3 reveals an additional information on a_L/a_H for mode mixing. In this particular case, all extrema of the low tone $F_L'(t)$ coincide with a portion of the extrema of the high tone $F_H'(t)$. This shortens all green regions into individual green points, where all extrema of $x(t)$ take place within. In order to avoid any unexpected extremum of $x(t)$ outside the green points, the requirement for $a_L/a_H > M_{max}$ in (5) has to be fulfilled over the gray regions $T_{opposite}$. As shown in Fig. 3, two M_{max} points of a same value appear right beside the instance of the green point between two gray regions. However, evaluating the value of M_{max} according to (4) results in an indeterminate form of 0/0 since the slopes of $F_L'(t)$ and $F_H'(t)$ are approximate to 0 at the two M_{max} points. Yet the limit of M_{max} may be derived using L'Hôpital's rule. Substituting the limit, $(f_H/f_L)^2$ in this case, for M_{max} into (5) leads to $a_L/a_H > (f_H/f_L)^2$. Thus, the analytic expression determines the range of mode mixing for the two-tone signal $x(t)$ on a $a_L/a_H - f_L/f_H$ plot. It can be imagined that different combinations of φ_H, f_H, f_L, and φ_L such that all extrema of the low tone coincide with a portion of the extrema of the high tone also lead to the same result. In these cases, the analytic expression also determines the boundary curve of the mode-mixing range as given by

$$\left(\frac{a_L}{a_H}\right)\left(\frac{f_L}{f_H}\right)^2 = 1. \tag{6}$$

It is worth noting that this curve agrees with the upper boundary curve in Rilling's map [17], as mentioned in section II-B. Table 1 shows symbols used through the paper and their corresponding definition.

TABLE 1. List of symbols used in this paper.

Symbol	Meaning
$x(t)$	two-tone composite
$F_L(t)$	low-tone component of a two-tone composite $x(t)$
$F_H(t)$	high-tone component of a two-tone composite $x(t)$
$m_L(t)$	slope of the low-tone component $F_L(t)$
$m_H(t)$	slope of the high-tone component $F_H(t)$
a_L	amplitude of the low-tone $F_L(t)$
a_H	amplitude of the high-tone $F_H(t)$
f_L	frequency of the low-tone $F_L(t)$
f_H	frequency of the high-tone $F_H(t)$
φ_L	initial phase of the low-tone $F_L(t)$
φ_H	initial phase of the high-tone $F_H(t)$
$T_{opposite}$	intervals in which the signs of $m_L(t)$ and $m_H(t)$ are opposite to each other but except for the green background region
M_{max}	the maximum value of $M(t)$ in the intervals of $T_{opposite}$ (gray background)

III. METHOD

A. SIMULATION

First, each of the two phases φ_L and φ_H is assigned a value. For simplicity, we can always shift both phases together so that $\varphi_L = 0$ and φ_H becomes a relative phase at all times. Second, the value of the finite maximum $M_{finite\ max}$ is calculated as a function of f_L/f_H at the fixed φ_H and $\varphi_L = 0$. Namely, the corresponding minimal amplitude ratio a_L/a_H $(= M_{max})$ to cause mode mixing is obtained according to (5). Third, repeating the same procedures for $0 \le \varphi_H < 2\pi$ gives

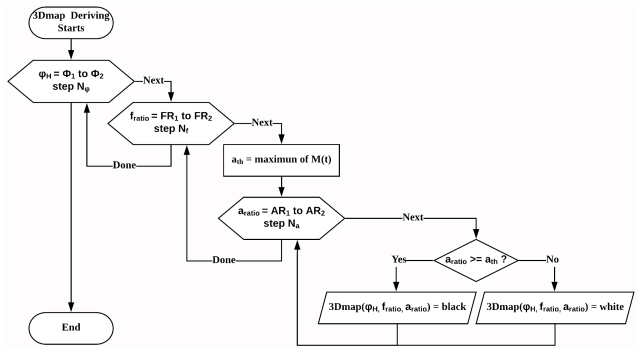

FIGURE 4. A computer flowchart for deriving our 3D map.

a reference to identify the mode mixing problem in a 3D space of the coordinate $\left(\log\left(a_L/a_H\right), f_L/f_H, \varphi_H\right)$. Namely, given with a set of values of the three parameters, one can affirm whether the two components are mixed according to the criterion. Last, a black/white 3D map is obtained, which plots the binary result of mode mixing in black or white as a function of the three parameters. Then, the position of the black/white 3D map within the black region indicates the presence of the mode mixing problem. Fig. 4 illustrates a computer flowchart for deriving our 3D map.

B. EXPERIMENT

The experimental validation of (5) as a criterion of mode mixing for a two-tone composite signal was demonstrated by using the decomposition of the CoM trajectory signals in EMD. In this study, 23 adults walked with wearable accelerometers on their lower backs for gait analysis [11]. All subjects provided informed written consent before participating in the study. The protocol was approved by the local human studies committee. The acceleration signal of each adult was detrended by EMD and then integrated with respect to time twice into a CoM displacement time series. Then, each CoM displacement time series was decomposed for an expected IMF with a dominant frequency of 1 Hz, which is the average oscillating frequency of the CoM trajectory in the ML direction of a healthy adult during walking. It is the particular IMF that is valid for gait analysis. In our study, the decomposition works for 17 out of the 23 CoM displacement time series but fails for the remaining six.

In the case of successful decomposition, the phenomenon of mode mixing is absent. For each of the 17 CoM displacement time series, the particular IMF due to walking and its neighboring IMF due to noises are first separated using EMD. The values of the two frequencies f_L and f_H, the two amplitudes a_L and a_H, and the two phases φ_L and φ_H of the two IMFs can be obtained through estimation, separately. We use the counting extrema method [26] to estimate the frequency of an IMF. Moreover, the amplitude of an IMF can be estimated through averaging the heights of all extrema. As for the initial phase, the normalized Hilbert transform [28] is used. After that, we shift both the estimated φ_H and φ_L together to obtain the relative phase φ'_H accompanying $\varphi'_L = 0$. For simplicity, we still denote the relative phase φ'_H as φ_H. Finally, a_L/a_H, f_L/f_H, and the relative phase φ_H of the particular IMF and the neighboring IMF are presented as the practicable decomposition results to be compared in our black/white 3D map. A symbol of "o" is marked at the coordinate $\left(\log\left(a_L/a_H\right), f_L/f_H, \varphi_H\right)$ in our map for each of the 17 series, individually. We expect that all the decomposition results without the mode mixing problem will be located inside the white region of the map.

In the case of mode mixing for the remaining six CoM displacement time series, the particular IMF due to walking and its neighboring IMF due to noises are mixed. Fortunately, the mixed IMFs can be separated using masking signal-assisted EMD [16], [19] instead. Similarly, the values of the frequencies, the amplitudes, and the phases of the two IMFs can be obtained, separately. Subsequently, a symbol of "x" is marked at the corresponding coordinate in our black/white 3D map for each of the six series, individually. All these six records located within the black region of the map are expected.

IV. RESULTS

A. BLACK/WHITE 3D MAP

According to the criterion of mode mixing as given by (5), Fig. 5(a) illustrates the black/white 3D map which plots the

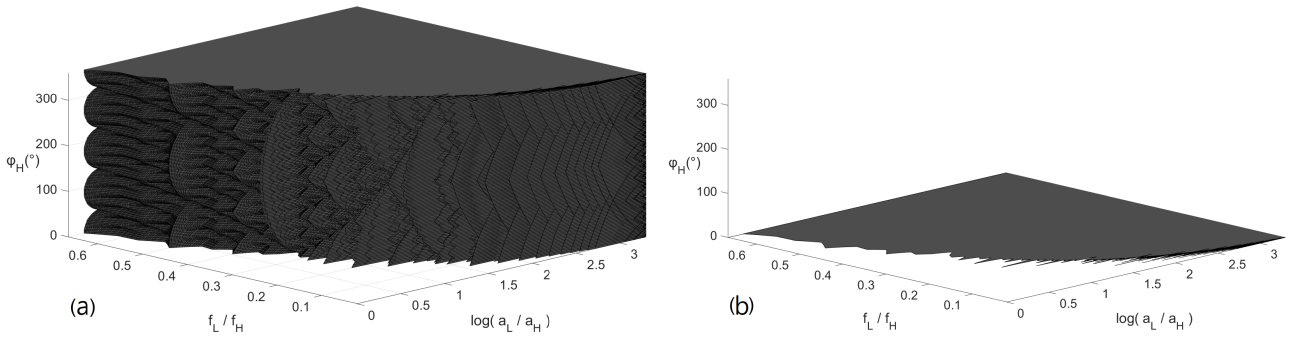

FIGURE 5. (a) The black/white 3D map in this study, which provides a clear vision for identifying the mode mixing problem of a two-tone signal. The position within the white region means the two-tone signal can be decomposed by EMD, and vice versa. (b) The cross section at $\varphi_H = 0$ of the black/white 3D map.

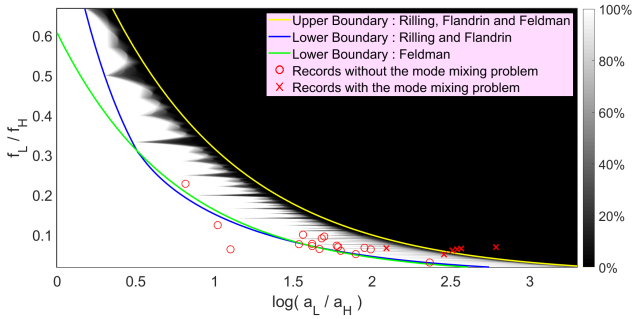

FIGURE 6. Normalized average of Fig. 5(a) onto $\log(a_L/a_H) - f_L/f_H$ plane. There are 17 and 6 records with the absence (symbol of "o") and presence (symbol of "x") of the mode mixing problem, respectively. According to the corresponding location, (5) is verified successfully by all the records. Moreover, the upper and lower boundaries derived from Rilling and Flandrin [17] and by Feldman [27] are also plotted.

binary result of mode mixing in black or white as a function of the amplitude ratio a_L/a_H, the frequency ratio f_L/f_H, and the relative phase φ_H between the two components of a two-tone signal $x(t)$. Fig. 5(b) shows a cross-section of the black/white 3D map at $\varphi_H = 0$. The black and the white regions in the map denote the presence and the absence of mode mixing, respectively. Note that the boundary between the two regions in Fig. 5(b) s irregular, which is similar to that in Rilling's *Boundary Condition Map*.

Fig. 6 shows a gray two-dimensional (2D) map. The 2D map was first an average of the black/white 3D map onto the $\log(a_L/a_H) - f_L/f_H$ plane and then normalized such that the pixels of the 2D map are in gray ranging from 0.0% to 100.0%. Herein, each pixel represents a coordinate on the map, which reveals the relation of a_L/a_H and f_L/f_H between the two components of a two-tone signal. Again, the black and the white areas indicate the presence and the absence of the mode mixing of the two components for all φ_H between 0.0 and 2π, respectively. However, the gray area implies that the mode mixing only occurs at some particular relative phases φ_H. It can be imagined that the grayer a pixel is, the more particular relative phases φ_H the pixel has, and the higher the probability of mode mixing. In other words, the degree of the gray color of a pixel suggests the probability of mode mixing to occur at the pixel as the relative phase φ_H is unavailable. This resembles the efficiency of separation for two-tone signals over the interspace in Rilling's *Boundary Condition Map*.

Figure 6 also shows the upper and the lower boundary curves in the *Boundary Condition Map* presented by Rilling, Flandrin [17] and Feldman [27]. It can be seen that the interspace between their upper and the lower boundary curves just coincides with the gray area in our gray 2D map. However, the occurrence of mode mixing in Rilling's interspace is statistically estimated in terms of the separation efficiency. On the contrary, the occurrence of mode mixing in our gray area can be affirmed once the relative phase φ_H is available.

B. MODE MIXING OF COM TRAJECTORY

The validation of the black/white 3D map is examined by using the experimental results obtained from our gait analysis. As seen in Fig. 6, there are 17 symbols of "o" within the white and the gray areas as well as 6 symbols of "x" within the black and the gray areas. Recall that each symbol "o" denotes a CoM trajectory time series that is free of mode mixing. On the contrary, each symbol "x" denotes a CoM trajectory time series that encounters mode mixing. As the 23 symbols were relocated into the black/white 3D map, the 17 symbols of "o" were found within the white region while the 6 symbols of "x" were found within the black region. Experimentally, the result agrees with our findings, as described in section III-B. Numerically, the result has been justified by applying (5), a criterion of mode mixing, to each of the 23 sets of CoM trajectory signals, individually.

V. CONCLUSION

Based on the findings by Rilling and Flandrin [17] and Feldman [27], we proposed a criterion for mode mixing separation in EMD, which provides a binary judgment on the mode mixing separation instead of the above efficiency of separation. According to the criterion, one can affirm whether or not the two components of a two-tone signal are mixed once the amplitude ratio, the frequency ratio, and the relative phase of the two components are given. Accordingly, a black/white 3D map was derived, which plots the binary result of mode mixing in black or white as a function of the three parameters. The black/white 3D map agrees with Rilling's *Boundary Condition Map* and the experiment results obtained from our gait analysis. Among the 23 sets of CoM trajectory signals, six sets encountered the mode mixing problem and their coordinates of the three parameters were found in the black region of the 3D map while the other 17 sets were in the white region. Therefore, our black/white 3D map provides a straightforward interpretation of the mode mixing problem in EMD. The criterion along with the interpretation will benefit the further development of EMD-related algorithms [16], [19], [21], [24], [29]–[31] for mode mixing separation.

ACKNOWLEDGMENT

The authors thank Jeffrey M. Hausdorff at the Tel Aviv Sourasky Medical Center for the database of CoM acceleration during walk.

REFERENCES

[1] M. S. Orendurff, A. D. Segal, G. K. Klute, J. S. Berge, E. S. Rohr, and N. J. Kadel, "The effect of walking speed on center of mass displacement," *J. Rehabil. Res. Dev.*, vol. 41, pp. 829–834, 2004.

[2] B.-J. Hsue, F. Miller, and F.-C. Su, "The dynamic balance of the children with cerebral palsy and typical developing during gait. Part I: Spatial relationship between COM and COP trajectories," *Gait Posture*, vol. 29, no. 3, pp. 465–470, 2009.

[3] V. Lugade, V. Lin, and L.-S. Chou, "Center of mass and base of support interaction during gait," *Gait Posture*, vol. 33, no. 3, pp. 406–411, 2011.

[4] M. J. Floor-Westerdijk, H. M. Schepers, P. H. Veltink, E. H. F. Van Asseldonk, and J. H. Buurke, "Use of inertial sensors for ambulatory assessment of center-of-mass displacements during walking," *IEEE Trans. Biomed. Eng.*, vol. 59, no. 7, pp. 2080–2084, Jul. 2012.
[5] R. C. González, D. Alvarez, A. M. López, and J. C. Alvarez, "Ambulatory estimation of mean step length during unconstrained walking by means of COG accelerometry," *Comput. Methods Biomech. Biomed. Eng.*, vol. 12, no. 6, pp. 721–726, 2009.
[6] N. E. Huang, Z. Shen, S. R. Long, M. C. Wu, H. H. Shih, Q. Zheng, N.-C. Yen, C. C. Tung, and H. H. Liu, "The empirical mode decomposition and the Hilbert spectrum for nonlinear and non-stationary time series analysis," *Proc. Roy. Soc. London A, Math., Phys. Eng. Sci.*, vol. 454, no. 1971, pp. 903–995, 1998.
[7] N. E. Huang, Z. Shen, and S. R. Long, "A new view of nonlinear water waves: The Hilbert spectrum," *Annu. Rev. Fluid Mech.*, vol. 31, pp. 417–457, Jan. 1999.
[8] W. S. Chan, Y. L. Xu, X. L. Ding, and W. J. Dai, "An integrated GPS–accelerometer data processing technique for structural deformation monitoring," *J. Geodesy*, vol. 80, no. 12, pp. 705–719, Nov. 2006.
[9] J. Hwang, H. Yun, S.-K. Park, D. Lee, and S. Hong, "Optimal methods of RTK-GPS/accelerometer integration to monitor the displacement of structures," *Sensors*, vol. 12, no. 1, pp. 1014–1034, Jan. 2012.
[10] N. E. Huang and S. S. P. Shen, *Hilbert–Huang Transform and Its Applications*, 2nd ed. Singapore: World Scientific, 2014.
[11] X. Cui, C.-K. Peng, M. D. Costa, A. Weiss, A. L. Goldberger, and J. M. Hausdorff, "Development of a new approach to quantifying stepping stability using ensemble empirical mode decomposition," *Gait Posture*, vol. 39, no. 1, pp. 495–500, Jan. 2014.
[12] Z. Jinping, "Study on the effects of abnormal events to empirical mode decomposition method and the removal method for abnormal signal," *J. Ocean Univ. Qingdao*, vol. 31, no. 6, pp. 805–814, 2001.
[13] J. Terrien, C. Marque, and B. Karlsson, "Automatic detection of mode mixing in empirical mode decomposition using non-stationarity detection: Application to selecting IMFs of interest and denoising," *EURASIP J. Adv. Signal Process.*, vol. 2011, no. 1, p. 37, Dec. 2011.
[14] B. Tang, S. Dong, and T. Song, "Method for eliminating mode mixing of empirical mode decomposition based on the revised blind source separation," *Signal Process.*, vol. 92, no. 1, pp. 248–258, Jan. 2012.
[15] O. B. Fosso and M. Molinas, "EMD mode mixing separation of signals with close spectral proximity in smart grids," in *Proc. IEEE PES Innov. Smart Grid Technol. Conf. Eur. (ISGT-Eur.)*, Oct. 2018, pp. 1–6.
[16] R. Deering and J. F. Kaiser, "The use of a masking signal to improve empirical mode decomposition," in *Proc. IEEE Int. Conf. Acoust., Speech, Signal Process. (ICASSP)*, vol. 4, Mar. 2005, pp. 485–488.
[17] G. Rilling and P. Flandrin, "One or two frequencies? The empirical mode decomposition answers," *IEEE Trans. Signal Process.*, vol. 56, no. 1, pp. 85–95, Jan. 2008.
[18] Z. Wu, N. E. Huang, and X. Chen, "The multi-dimensional ensemble empirical mode decomposition method," *Adv. Adapt. Data Anal.*, vol. 01, no. 03, pp. 339–372, Jul. 2009.
[19] C. Wang and F. Da, "Differential signal-assisted method for adaptive analysis of fringe pattern," *Appl. Opt.*, vol. 53, no. 27, pp. 6222–6229, Sep. 2014.
[20] Y.-H. Wang, H.-W. V. Young, and M.-T. Lo, "The inner structure of empirical mode decomposition," *Phys. A, Statist. Mech. Appl.*, vol. 462, no. 300, pp. 1003–1017, 2016.
[21] C. Wang, Q. Kemao, and F. Da, "Regenerated phase-shifted sinusoid-assisted empirical mode decomposition," *IEEE Signal Process. Lett.*, vol. 23, no. 4, pp. 556–560, Apr. 2016.
[22] G. Xu, Z. Yang, and S. Wang, "Study on mode mixing problem of empirical mode decomposition," in *Proc. Joint Int. Inf. Technol., Mech. Electron. Eng. Conf.*, 2016, pp. 389–394.
[23] F. M. Z. Bahri and J. J. Sharples, "Empirical Mode Decomposition and two-tone separation problem in the presence of noise," in *Proc. 22nd Int. Congr. Modelling Simulation*, 2017, pp. 167–173.
[24] H.-W. Yang, S.-K. Jeng, H.-W. V. Young, C. Lin, Y.-H. Wang, K. Hu, and M.-T. Lo, "A minimum arclength method for removing spikes in empirical mode decomposition," *IEEE Access*, vol. 7, pp. 13284–13294, 2019.
[25] S. S. P. Shen, T. Shu, N. E. Huang, Z. Wu, G. R. North, T. R. Karl, and D. R. Easterling, "HHT analysis of the nonlinear and non-stationary annual cycle of daily surface air temperature data," in *Hilbert–Huang Transform and Its Applications*, N. E. Huang and S. S. P. Shen, Eds., 2nd ed. Singapore: World Scientific, 2014, pp. 261–283.
[26] N. E. Huang and S. S. P. Shen, "Statistical significance test of intrinsic mode functions," in *Hilbert–Huang Transform and Its Applications*, N. E. Huang and S. S. P. Shen, Eds., 2nd ed. Singapore: World Scientific, 2014, pp. 149–169.
[27] M. Feldman, "Analytical basics of the EMD: Two harmonics decomposition," *Mech. Syst. Signal Process.*, vol. 23, no. 7, pp. 2059–2071, Oct. 2009.
[28] N. E. Huang and S. S. P. Shen, "Introduction to the Hilbert–Huang transform and its related mathematical problems," in *Hilbert–Huang Transform and Its Applications*, N. E. Huang and S. S. P. Shen, Eds., 2nd ed. Singapore: World Scientific, 2014, pp. 1–26.
[29] Z. Wu and N. E. Huang, "Ensemble empirical mode decomposition: A noise-assisted data analysis method," *Adv. Adapt. Data Anal.*, vol. 01, no. 01, pp. 1–41, Jan. 2009.
[30] F. Xu, X. Song, K.-L. Tsui, F. Yang, and Z. Huang, "Bearing performance degradation assessment based on ensemble empirical mode decomposition and affinity propagation clustering," *IEEE Access*, vol. 7, pp. 54623–54637, 2019.
[31] T. Jin, Q. Li, and M. A. Mohamed, "A novel adaptive EEMD method for switchgear partial discharge signal denoising," *IEEE Access*, vol. 7, pp. 58139–58147, 2019.

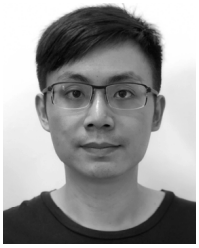

HAN-PING HUANG was born in Yilan, Taiwan, in 1986. He received the M.S. degree in electrophysics from National Chiao Tung University, Hsinchu, Taiwan, in 2010, where he is currently pursuing the Ph.D. degree. He is also with the Department of Electrophysics, National Chiao Tung University. His current research interests include, but are not limited to, physiological signal analysis, signal processing, and related interdisciplinary research topics.

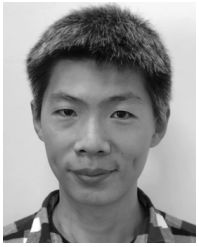

SUNG-YANG WEI was born in New Taipei City, Taiwan, in 1982. He received the M.S. degree in electrophysics from National Chiao Tung University, Hsinchu, Taiwan, in 2010, where he is currently pursuing the Ph.D. degree with the Department of Electrophysics. His current research interests include, but are not limited to, biomedical image processing and physiological signal complexity analysis.

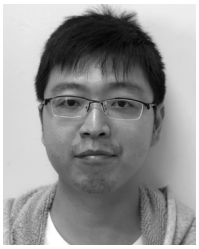

HSUAN-HAO CHAO was born in Tainan, Taiwan, in 1988. He received the M.S. degree in electrophysics from National Chiao Tung University, Hsinchu, Taiwan, in 2012, where he is currently pursuing the Ph.D. degree with the Department of Electrophysics. His current research interests include, but are not limited to, biomedical physics and signal processing.

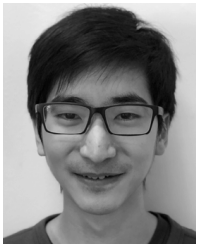

CHANG FRANCIS HSU was born in Boston, MA, USA, in 1992. He received the B.S. degree in physics from National Tsing Hua University, Hsinchu, Taiwan, in 2015. He is currently pursuing the Ph.D. degree with the Department of Electrophysics, National Chiao Tung University. His current research interests include, but are not limited to, biological complexity, fluid mechanics, and machine learning.

LONG HSU was born in Kaohsiung, Taiwan, in 1958. He received the M.S. degree from New Mexico State University, NM, USA, in 1986, and the Ph.D. degree from the Massachusetts Institute of Technology School, MA, USA, in 1994. His research interests include biophysics and physiological signal analysis.

Since 1995, he has been an Associate Professor with National Chiao Tung University.

SIEN CHI was born in Jiangsu, China, in 1936. He received the B.S.E.E. degree from National Taiwan University, Taipei, Taiwan, in 1959, the M.S.E.E. degree from National Chiao Tung University, Hsinchu, Taiwan, in 1961, and the Ph.D. degree in electrophysics from Polytechnic Institute, Brooklyn, NY, USA, in 1971. His research interests include optical-fiber communications, fast and slow light, passive optical networks, microwave photonics, and physiological signal analysis.

From 1971 to 2004, he was a Professor with National Chiao Tung University, where he was also the Vice President, from 1998 to 2001, and he is currently a Chair Professor.

Dr. Chi is also a Fellow of the Optical Society of America.